Received: 7 January 2017 | Revised: 21 August 2017 | Accepted: 8 January 2018

DOI: 10.1002/stc.2149

RESEARCH ARTICLE

WILEY

Observer-based repetitive model predictive control in active vibration suppression

Atta Oveisi[1] | Mehran Hosseini-Pishrobat[2] | Tamara Nestorović[1] | Jafar Keighobadi[2]

[1] Institute of Computational Engineering, Ruhr-Universität Bochum, Universitätsstr. 150, D-44801 Bochum, Germany

[2] Department of Mechanical Engineering, University of Tabriz, 29 Bahman, Tabriz, Iran

Correspondence
Atta Oveisi, Institute of Computational Engineering, Ruhr-Universität Bochum, Universitätsstr. 150, D-44801 Bochum, Germany.
Email: atta.oveisi@rub.de

Summary

In this paper, an observer-based feedback/feedforward model predictive control (MPC) algorithm is developed for addressing the active vibration control (AVC) of lightly damped structures. For this purpose, the feedback control design process is formulated in the framework of disturbance rejection control (DRC) and a repetitive MPC is adapted to guarantee the robust asymptotic stability of the closed-loop system. To this end, a recursive least squares (RLS) algorithm is engaged for online estimation of the disturbance signal, and the estimated disturbance is feed-forwarded through the control channels. The mismatched disturbance is considered as a broadband energy bounded unknown signal independent of the control input, and the internal model principle is adjusted to account for its governing dynamics. For the sake of relieving the computational burden of online optimization in MPC scheme, within the broad prediction horizons, a set of orthonormal Laguerre functions is utilized. The controller design is carried out on a reduced-order model of the experimental system in the nominal frequency range of operation. Accordingly, the system model is constructed following the frequency-domain subspace system identification method. Comprehensive experimental analyses in both time-/frequency-domain are performed to investigate the robustness of the AVC system regarding the unmodeled dynamics, parametric uncertainties, and external noises. Additionally, the spillover effect of the actuation authorities and saturation of the active elements as two common issues of AVC systems are addressed.

KEYWORDS

disturbance estimation, model predictive control, orthonormal basis functions, piezoelectric material, vibration attenuation

1 | INTRODUCTION

Model predictive control (MPC) is an optimization-based method in which, the control inputs are obtained by solving a set of finite-horizon optimal control problems successively over the sampling instants. The optimal control formulation of the MPC explicitly takes into account model-based predictions of the controlled system trajectories. The obtained solutions of the optimal control problems are concatenated in a receding horizon framework, to construct the MPC feedback law. By the advances of embedded computer processors along with the enhanced optimization solvers, the MPC methods are appearing more and more in the emerging industrial applications.[1] In comparison with the other industrial control

technologies, such as proportional-integral-derivative (PID) control, the distinguishing features of MPC are[2] (a) MPC has an inherent capability of taking into account the hard constraints on the system, such as actuator saturation. (b) MPC algorithms offer an optimal systematic framework for handling multi-input-multi-output systems. The practical advantages of MPC over the PID approach were investigated widely in the literature.[3] MPC can handle multi-objective performance requirements in multi-input-multi-output systems, whereas the multiple PID compensators are hard to tune. Additionally, compared with the classic optimal, robust, and robust multi-objective controllers, MPC is the only candidate that efficiently incorporates actuator limitations such as saturation, the rate-of-change constraints, and even plant output amplitude constraints. For instance, as pointed out by Wai et al., in structural control of wind turbines, maximizing the power production while keeping the fatigue forces minimal are contradictive objectives on the actuation force which cannot be handled by PID, linear quadratic Gaussian (LQG), and classical H_∞ controllers.[4]

In another application, for example, the AVC of flexible manipulators, constraints on the system outputs such as the maximum oscillation level will imply the reduction of the overall structural stress level which can be realized by MPC.[5] In the context of these manipulators, the lightweight elastic links are replacing the bulky ones which are important in robotics and aerospace applications. For instance, the International Space Station has significantly contributed to this area, e.g., Canadarm2 and European Robotic Arm.[6] Although both of these examples are manufactured from carbon fiber composite materials, oscillations in their arm-tip are inevitable due to their beam-like geometries. Owing to the fast dynamics of such lightly damped mechanical systems, the implementation of a MPC requires large optimization horizons. However, a broad horizon increases the dimension of the MPC optimization vector, precluding the application of the method under high sampling speeds. To address this issue, the control variables along the optimization horizon are parameterized by a finite set of orthonormal basis functions.[2,7] On the other hand, asymmetric dynamical loads in practical applications as the consequence of periodic repetitive disturbances are unavoidable. Consequently, the information on the repetitive pattern of the disturbance signal is incorporated in the synthesis process of MPC.[8] Following the aforementioned constraints on the flexible links, in this paper, we are interested in "end-effector regulation" problem as well as constraint-time "rest-to-rest motion".[9] It should be emphasized that we are dealing with local vibration suppression in contrast to the selective mode shape control scheme.[10] However, considering the geometry of the structure, that is, smart cantilever beam (see Figure 1a), the transient response mostly depends on the dominant set of transverse modes. Therefore, suppressing the vibration at the free end of the beam results in global attenuation. This justifies the use of "end-effector regulation" in the context of this paper. The constraints on the end-effector regulation problem are directly related to the global damping ratio and the exponential decay rate of the closed-loop system.

The appropriate control signals, which satisfies these performance objectives, may be realized by use of piezo-actuators in the context of smart structures.[11,12] These structural configurations are additionally employed to control the stress, strain, and sound.[13–15] Consequently, by utilizing suitable sensor elements, the undesired environmental disturbances can be rejected.[16–18] Hassan et al. presented a remarkable survey of the application of piezo-actuators/sensors in AVC.[19] An important step in the AVC of smart structures is the mathematical modeling as the base of controller/observer design. Although there are a large number of exact and numerical linear and nonlinear methods for modeling of the structures, they are mostly limited to some simple geometries including beam, plate, and panel with ideal boundary conditions.[20,21] Therefore, a system identification approach as a more practical method is introduced to extract the dynamical model where analytical/numerical methods are missing. As expected, the identification methods introduce various sorts of uncertainties such as structured uncertainty and unmodeled dynamics, which should be addressed by the controller and observer systems.[22]

In the recent two decades, various control techniques based on the linear quadratic regulator (LQR), LQG, and robust control (H_∞- and μ-synthesis) have been widespread in the literature. However, the application of such benchmarks is rarely adopted in the industry.[4] Actuator saturation or bandwidth limitations in the nominal frequency range of the plant, which are ignored in these methods, are two main reasons for this matter. As pointed out by Njiri and Söffker,[23] violations of these constraints may cause various technical difficulties, for example, windup problem. To the modest knowledge of the authors, other than MPC, only antiwindup compensation in augmentation with linear control is available as a systematical solution for actuator saturation problems.[24,25] However, in comparison to MPC, in which the hard constraints are included in the online optimization of the control synthesis, in the antiwindup framework, the system should be subjected to actuation nonlinearities in real time so that an additional compensator becomes active.[26] Moreover, updating the transducers to include a greater dynamic range decreases the signal-to-noise ratio and reduces the time resolution not mentioning the physical size limitations as well as the cost of new transducers.[27] Consequently, the MPC is known to be the control strategy that can include various explicit process constraints. This feature motivates tackling the AVC using MPC.[28–30] Despite the limiting requirement for fast

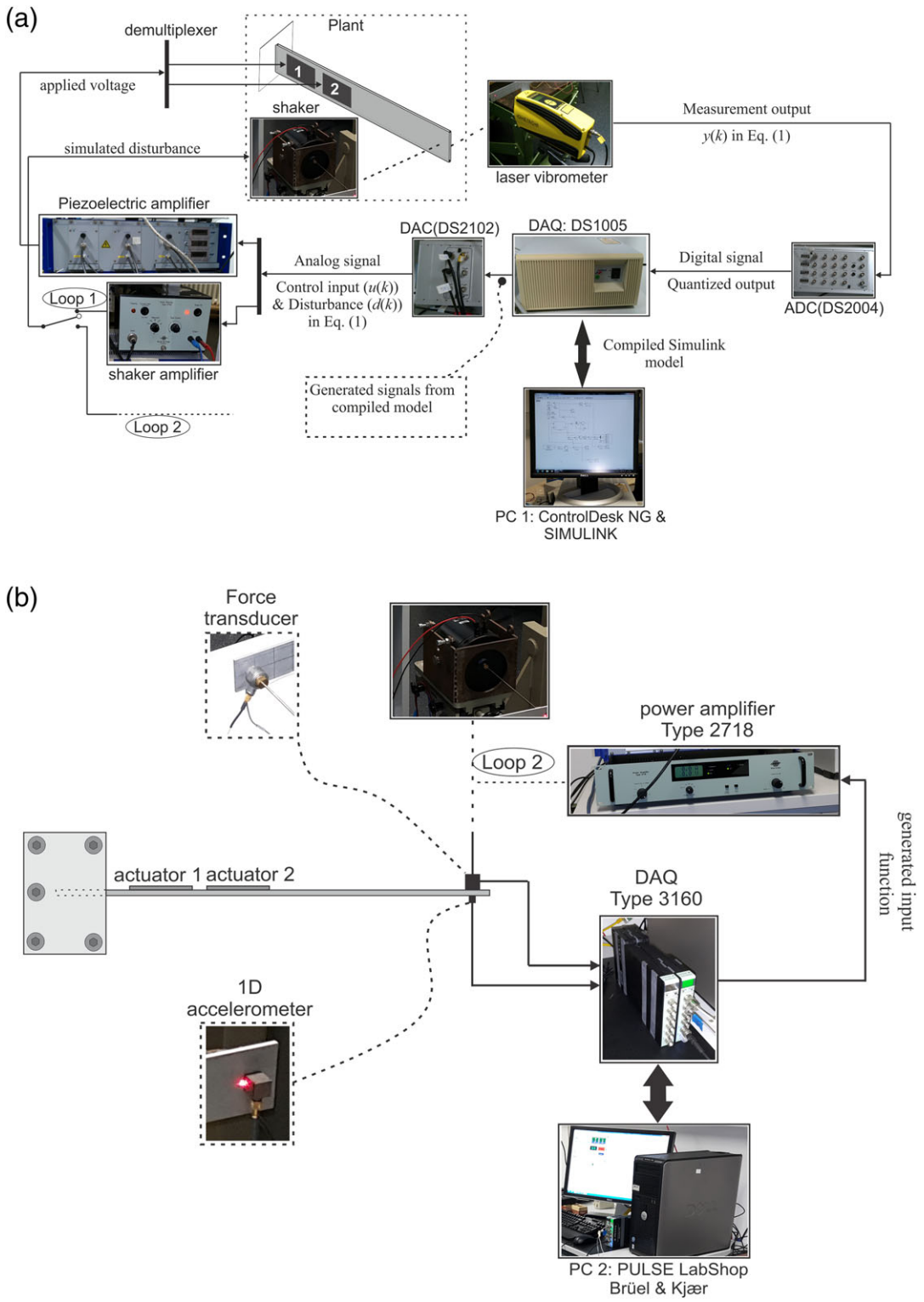

FIGURE 1 (a) Experimental rig of control loop. (b) Experimental setup for modal analysis

sampling which is known as the main drawback of MPC in AVC applications, it is shown in this paper that the proposed method is fast enough to overcome this problem even in high frequencies of disturbance signal. Finally, the application of MPC in nonlinear systems is mostly neglected in literature.[31,32]

This paper contributes to the development of a repetitive MPC based on the internal model principle (IMP) and disturbance estimation together with practical consideration of implementing the MPC in AVC. Accordingly, a memory records the plant output and a time-shifter shifts the states of the estimator forwards in time to generate the appropriate

control action in disturbance rejection control (DRC). It should be mentioned that AVC effectively operates in an approximate bandwidth of 1 kHz (in this paper 800 Hz) and higher frequency ranges are mostly treated by passive methods.[27] The rest of the paper is organized as follows: In Section 2, the problem is defined and the proposed control system is introduced. To verify the performance of the control system, it is implemented on a real-time vibrating system. The experimental configuration and mathematical modeling are carried out in Section 3. The numerical investigations of the implementation of the proposed controller on the vibrating structure are studied in Section 4 in detail.

2 | CONTROL STRATEGY

In this section, first, the classical MPC method based on IMP is presented for a discrete linear time-invariant (LTI) system in the state space form. Next, the repetitive control strategy is presented to account for periodic DRC. The control problem is then formulated in the form of optimal feedback controller synthesis for the augmented plant. The hard actuator constraints, as side conditions on the optimization problem, are reinforced in each time interval in an online manner.[33] Various improvements are considered for enhancing the stability and performance of standard control system as well as the numerical solution for the optimization problem in Subsections 2.3 through 2.5.

2.1 | MPC design

An observer-based MPC as a model-based control strategy uses the current control input and the observed states of the plant (and possibly the estimation of disturbance) to simultaneously predict the future output of the plant and the control signal in a finite horizon. The underlying system is modeled by the following finite dimensional, discrete-time state space representation through a lumped parameter approximation

$$x(k+1) = Ax(k) + Bu(k) + Hd(k), y(k) = Cx(k). \tag{1}$$

The vector, $x(.) \in \mathbf{R}^n$ is the state, $u(.) \in \mathbf{R}^m$ is the control input, $y(.) \in \mathbf{R}^p$ is the measurement vector, and $d(.) \in \mathbf{R}^r$ denotes the unknown, mismatched disturbance signal. It is assumed that the pair (A, B) is stabilizable, and (C, A) is detectable. The dimensions of the state, input, and output vectors are selected based on the results of the system identification problem in Section 3. The system matrices A, B, C, and H are given in Appendix A for the continuous time counterpart of Equation (1). The admissible control inputs are characterized by a compact set, $\mathcal{U} := \{u \in \mathbf{R}^m \mid |u_i| \leq u_{i0}, i = 1, ..., m\}$, in which u_{i0} are strictly positive numbers specifying the saturation limits of the actuators. The class of mechanical disturbances, $d(.)$, is assumed to be generated by an autonomous dynamic system of the form (2),[34]

$$w(k+1) = Sw(k), d(k) = Ew(k), \tag{2}$$

where $w(.) \in \mathbf{R}^{n_w}$ is the state vector and S and E are real matrices of appropriate dimensions. It is assumed that the eigenvalues of the matrix S belong to the unit disk in the complex plane, that is, $|z| \leq 1$. Besides, the eigenvalues which lie on the boundary $|z| = 1$ are simple. This assumption ensures that the nonvanishing components of the disturbance are bounded and periodic.[35] Accordingly, the eigenvalues of S capture the dominant frequency characteristics of the disturbance signal. The characteristic polynomial of S is considered as

$$\Gamma(z) := \det(zI - S) = z^{n_w} + \sum_{i=1}^{n_w} \alpha_i z^{n_w - i}.$$

In this paper, a repetitive control framework is introduced into the MPC system for disturbance rejection. The repetitive control systems provide an operational means for rejection of periodic disturbances based on IMP.[36] The term "repetitive" accentuates the periodic nature of the signals to be rejected. By IMP, asymptotic disturbance rejection in a control system amounts to incorporating a suitable dynamic generator (of the disturbances) in the closed-loop system.[37] Using an internal model, the controller replicates the repetitive characteristics of the disturbance signals in its structure. Consequently, the dynamic model of disturbance allows the controller to reject the disturbance signal with a proper elimination of the counteracting energy. To this end, the following causal operator corresponding to the characteristic polynomial $\Gamma(q^{-1})$ is considered as

$$\Gamma\left(q^{-1}\right) = 1 + \sum_{i=1}^{n_w} \alpha_i q^{-i}, \tag{3}$$

where q^{-1} denotes the backward shift operator.

Remark 1. In accordance with the characteristic equation of S in Equation (2), the following equality is deduced, $\Gamma(q^{-1})d(k) \equiv 0$.

The following filtered variables are introduced to embed the internal model of the disturbance signal into the control system:

$$\begin{aligned} x_f(k) &:= \Gamma\left(q^{-1}\right)x(k), \\ u_f(k) &:= \Gamma(q^{-1})u(k). \end{aligned} \tag{4}$$

In view of Remark 1, applying the operator $\Gamma(q^{-1})$ to the system Equation (1) yields Equation (5);

$$\begin{aligned} x_f(k+1) &= Ax_f(k) + Bu_f(k), \\ y(k) + \sum_{i=1}^{n_w} \alpha_i y(k-i) &= Cx_f(k). \end{aligned} \tag{5}$$

Setting $X(k) := \left[x_f^T(k), y^T(k-1), y^T(k-2), ..., y^T(k-n_w)\right]^T \in \mathbf{R}^{n+pn_w}$, we describe both filtered state and output equations by the following augmented system:

$$\begin{aligned} X(k+1) &= A_{aug}X(k) + B_{aug}u_f(k), \\ y(k) &= C_{aug}X(k), \end{aligned} \tag{6}$$

where the system matrices are given by

$$A_{aug} = \begin{bmatrix} A & O & O & \cdots & O \\ C & -\alpha_1 I & -\alpha_2 I & \cdots & -\alpha_{n_w} I \\ O & I & O & \cdots & O \\ \vdots & \vdots & \ddots & & \vdots \\ O & O & \cdots & I & O \end{bmatrix}, B_{aug} = \begin{bmatrix} B \\ O \\ O \\ \vdots \\ O \end{bmatrix},$$

$$C_{aug} = [C \ -\alpha_1 I \ -\alpha_2 I \ \cdots \ -\alpha_{n_w} I].$$

Remark 2. To guarantee the controllability and observability of the augmented system (6), we assume that the matrix

$$\begin{bmatrix} zI - A & B \\ -C & O \end{bmatrix},$$

is full rank for all z satisfying $\Gamma(z) = 0$. That is, the original system (1) has no common transmission zeros with the eigenvalues of the disturbance model.[38] The eigenvalues of matrix A_{aug} comprise those of A and a companion block matrix corresponding to the disturbance dynamics.[7] Thereby, in view of IMP, the repetitive DRC reduces to stabilization problem of the augmented system (6).[34]

2.2 | Repetitive MPC

To control the augmented system (6), an optimal feedback strategy is employed in the framework of predictive control. In this regard, at sampling instant k, the following finite horizon optimal control problem is solved to obtain the control action;

$$\min_{u_f(k+.|k)} \left\{ J(k) := \sum_{j=1}^{N} \beta^{-2j} \left| |X(k+j|k)|\right|_Q^2 + \beta^{-2(j-1)} \left| \left| u_f(k+j-1|k) \right| \right|_R^2 \right\}, \tag{7}$$

subject to

$$\begin{aligned} &X(k+j|k) = A_{aug}X(k+j-1|k) + B_{aug}u_f(k+j-1|k), \\ &X(k|k) = \widehat{X}(k), \\ &u_f(k+j-1|k) \in \mathcal{U}_f, \ j = 1, ..., N. \end{aligned}$$

In the formulation of Equation (7), N is a positive integer specifying the optimization horizon, $\beta > 1$ is the data weighting parameter, and $Q \succcurlyeq 0$ and $R \succ 0$ are performance weight matrices penalizing the pertinent variables. The

set $\mathcal{U}_f$ denotes the image of $\mathcal{U}$ under the filtering map $\Gamma(q^{-1})$. The vectors, $X(k+.|k)$ and $u_f(k+.|k)$, respectively stand for the predicted state and control variables along the optimization horizon. It should be pointed out that compared with the linear quadratic regulator on output (LQRY), which is mostly implemented in structural vibration control based on the steady state solution of algebraic Riccati equation (ARE), the repetitive MPC is the solution of online optimization of the closed-loop trajectory. To sum up, the low computational burden of linear MPC and its robustness features make it as a logical candidate compared with LQRY.[39,40] Also, the conservativeness of the LQR and LQG controllers by tuning the weighting matrices in solving the stage cost has been reported by Bossi et al.[10]

In Equation (7), the predictions are obtained through system dynamics with the recent state vector information as the initial value. Because the state vector $X(.)$ is not measured, an observer is used to asymptotically reconstruct the state information. To this end, the Kalman filter is employed owing to its optimal performance in noisy environments. The filter dynamics is governed by the following equations:[37]

$$\begin{aligned}
&\widehat{X}(k+1) = A_{aug}\widehat{X}(k) + B_{aug}u_f(k) + K_f(k)\Big(y(k) - C_{aug}\widehat{X}(k)\Big),\\
&\widehat{X}(0) = 0,\\
&K_f(k) = A_{aug}P_f(k)C_{aug}^T\Big(C_{aug}P_f(k)C_{aug}^T + R_f\Big)^{-1},\\
&P_f(k+1) = A_{aug}\big(I - K_f(k)C_{aug}\big)P_f(k)A_{aug}^T + Q_f,\\
&P_f(0) = P_{f0} \succ 0.
\end{aligned} \tag{8}$$

The matrix $P_f(.) \in \mathbf{R}^{(n+pn_w)\times(n+pn_w)}$ is the estimation error covariance, $Q_f \in \mathbf{R}^{(n+pn_w)\times(n+pn_w)}$ is the process noise covariance, $R_f \in \mathbf{R}^{p\times p}$ is the measurement noise covariance, and $K_f(.) \in \mathbf{R}^{(n+pn_w)\times p}$ denotes the gain of the filter. To alleviate the computational burden of the control method for AVC applications, the gain matrix $K_f(.)$ can be computed offline and stored in the memory for real-time implementations.[37] Solving the open-loop optimal control problem (7) over the sampling instants yields a receding horizon output feedback given by

$$u_f(k) = u_f^*(k|k), \tag{9}$$

in which $u_f^*(k|k)$ is the first element of

$$\Big\{u_f^*(k+j-1|k)\Big\}_{j=1}^{N} := \arg\min_{u_f(k+.|k)\in\mathcal{U}_f} J(k) \tag{10}$$

The weighting parameter β in the optimal control formulation (7) is used to assign an exponentially decreasing weight to the sequence of predicted system variables. The data weighting technique resolves the ill-conditioning problem of the Hessian matrix associated with $J(.)$ for large optimization horizons.[41] To render the optimization problem (7) to an optimal control problem with a time-invariant cost function, the following theorem is given.

Theorem 1. ([41]) The optimization problem in Equation (11) is equivalent to the one in Equation (7);

$$\min_{u_f^\beta(k+.|k)} \left\{ J_\beta(k) := \sum_{j=1}^{N} \Big|\Big|X_\beta(k+j|k)\Big|\Big|_Q^2 + \Big|\Big|u_f^\beta(k+j-1|k)\Big|\Big|_R^2 \right\}, \tag{10}$$

Subject to

$$\begin{aligned}
&X_\beta(k+j|k) = \frac{A_{aug}}{\beta}X_\beta(k+j-1|k) + \frac{B_{aug}}{\beta}u_f^\beta(k+j-1|k),\\
&X_\beta(k|k) = \beta^{-1}\widehat{X}(k),\\
&\beta^{j-1}u_f^\beta(k+j-1|k) \in \mathcal{U}_f,\ j = 1,\ldots,N
\end{aligned} \tag{11}$$

where

$$\begin{aligned}
&X_\beta(k+j|k) = \beta^{-j}X(k+j|k),\\
&u_f^\beta(k+j-1|k) = \beta^{-(j-1)}u_f(k+j-1|k),\ j = 1,\ldots,N.
\end{aligned} \tag{12}$$

Proof The proof directly follows from substituting the transformed variables (12) into the optimization problem (7).

□

Owing to Theorem 1, numerical optimization of the weighted repetitive MPC (7) is carried out based on the time-invariant cost function, $J_\beta(.)$ along with the associated scaled system dynamics. It should be noted that the present method compared with[27] is developed based on the IMP and a set of orthonormal Laguerre functions that alleviate the computational burden of online optimization. However,[27] is based on the traditional method of solving the optimization based on standard active set method. Finally, as another alternative,[42] an explicit-MPC within a broad prediction horizon, employs a multiparametric programming approach to create an offline lookup table and the resulted implementation is computationally inexpensive.[43]

2.3 | Numerical optimization via input parameterization

It is often required to use a large optimization horizon in MPC systems to achieve a satisfactory transient response and stability margin. The exponential data weighting technique removes the numerical ill-conditioning issue of the associated optimization. However, the dimension of the problem still could be large to be solved in fast sampling rates. A possible approach to remedy this issue and to reduce the size of the MPC synthesis is to parameterize the predicted control variables by a finite set of basis functions.[2] By this method, solving the optimal control problem (7) for the minimizing sequence, $\left\{u_f^*(k+j-1|k)\right\}_{j=1}^{N}$, boils down to finding the optimal parameterization coefficients in a lower dimension. Considering the linear and time-invariant characteristics of the underlying system (6), the exponential functions can approximate the stabilizing control inputs. In this regard, a class of orthonormal exponential basis functions, known as the Laguerre functions are used. The Laguerre functions are powerful approximation tools used in various fields such as system identification and signal processing.[44] A Laguerre basis of dimension N_ℓ and convergence rate of $a \in (0,1)$, also known as the scale factor of the Laguerre basis, is constructed in the frequency domain as follows

$$\mathcal{L}_i(z) := \frac{\sqrt{1-a^2}}{z-a}\left(\frac{1-az}{z-a}\right)^{i-1}, i = 1, ..., N_\ell. \tag{13}$$

In time-domain, the Laguerre functions are defined as the inverse z-transform of their frequency domain counterparts

$$\ell_i(k) := Z^{-1}\{\mathcal{L}_i(z)\}, i = 1, ..., N_\ell. \tag{14}$$

The orthonormality of the Laguerre functions can be represented as

$$\sum_{k=0}^{\infty} \ell_i(k)\ell_j(k) = \delta_{ij}, \tag{15}$$

where δ_{ij} is the Kronecker delta. To parameterize the predicted control sequence along the optimization horizon, a Laguerre basis of dimension N_i and pole a_i, denoted as $\left\{\ell_m^i(.)\right\}_{m=0}^{N_i}$, is designated to the i-th input $u_{f,i}^\beta(.)$. Accordingly, the following linear parameterization is considered:

$$u_{f,i}^\beta(k+p|k) = L_i^T(p)\eta_i, \quad p = 0, ..., N-1, \tag{16}$$

in which $L_i(.) := \left[\ \ell_1^i(.) \quad \cdots \quad \ell_{N_i}^i(.)\ \right]^T \in \mathbf{R}^{N_i}$ and $\eta_i \in \mathbf{R}^{N_i}$ denotes the pertinent parameterization vector. Using the input parameterization (16), Equation (11) is settled to the optimization problem in Equation (17);

$$\begin{aligned} &\min_{\eta}\left\{\eta^T R_\ell \eta + \sum_{j=1}^{N}\left|\left|X_\beta(k+j|k)\right|\right|_Q^2\right\}, \\ &\text{subject to} \\ &X_\beta(k+j|k) = \frac{A_{aug}}{\beta}X_\beta(k+j-1|k) + \frac{B_{aug}}{\beta}L^T(j-1)\eta, \\ &X_\beta(k|k) = \beta^{-1}\widehat{X}(k), \\ &\eta \in \Pi, j = 1, ..., N \end{aligned} \tag{17}$$

where

$$L(.) := \mathrm{diag}(L_1(.), ..., L_m(.)) \in \mathbf{R}^{\left(\sum_{i=1}^{m} N_i\right) m},$$
$$\eta := \mathrm{col}(\eta_1, ..., \eta_m) \in \mathbf{R}^{\sum_{i=1}^{m} N_i},$$
$$R_\ell := \sum_{j=1}^{N} L(j-1) R L^T(j-1).$$

The compact set $\Pi \subset \mathbf{R}^{\sum_{i=1}^{m} N_i}$ characterizes the feasible region for the parameterization vector, determined by the control constraint set. The primary control input u is confined to the box constraint set, $\mathcal{U}$ and thereby, the compact set Π can be represented by finite numbers of linear inequalities. As a result, the optimization problem (17) becomes a standard quadratic programming (QP) that can be solved efficiently in small sampling intervals. The MPC formulation (11) comprises an optimization problem of dimension Nm to obtain the current control action. The parameterization procedure converts this optimization problem to that of (17) with the dimension of $\sum_{i=1}^{m} N_i$. By the proper selection of the locations of the poles a_i, the predicted control trajectories can be effectively captured by the Laguerre approximation (16) with a few terms. This, in turn, considerably reduces the computational burden of the repetitive MPC and enables fast sampling rates for AVC applications.

2.4 | Stability analysis

A number of ways and means have been proposed in the literature to establish the Lyapunov stability of predictive optimal control schemes.[45,46] A majority of these methods impose fictitious state constraints to ensure that the optimal value of the MPC cost function decreases monotonically over the sampling instants. Predictive control formulations with terminal equality/inequality constraints are the most prominent representatives of these methods. However, such techniques for addressing the closed-loop stability often increase the computational burden and complexity of the associated optimization problem, precluding their applicability for fast sampling rates. Primbs and Nevistic[47] showed that, for a given MPC formulation, there exists a finite horizon for which the stability properties of the associated infinite horizon optimal control problem is retrieved. From such a perspective, Wang discussed the stability of the Laguerre approximation-based MPC in the framework of dual mode control.[2] Given the results from,[47] for a sufficiently large prediction horizon, the unconstrained solution of the optimal control problem (11) converges to that of the associated infinite horizon LQ control. When the constraints are active, the optimal control sequence satisfies the constraints along the optimization horizon for N_0 number of samples with $N_0 < N$. Then, the control sequence returns to the infinite horizon optimal solution that guarantees the closed-loop stability.

2.5 | Repetitive MPC with prescribed degree of stability

The exponential data weighting combined with the Laguerre parameterization offers a practical computational framework for handling large optimization horizons and, thereby, for recovering the infinite horizon control solutions. Accordingly, the stability results of LQR can be extended to the case of receding horizon control. In particular, to achieve a prescribed degree of stability, it is proposed to use the following weight matrices:

$$Q = \frac{\gamma^2}{\beta^2}\overline{Q} + \left(1 - \frac{\gamma^2}{\beta^2}\right) P_\infty, \quad R = \frac{\gamma^2}{\beta^2}, \tag{18}$$

in which $\gamma \in (0,1)$ is the required stability margin, $\overline{Q} \geqslant 0$, $\overline{R} > 0$, and P_∞ denote the solution of the following Riccati equation:

$$A_{aug}^T \left(P_\infty - \frac{1}{\beta^2} P_\infty B_{aug} \left(\overline{R} + \frac{1}{\gamma^2} B^T P_\infty B \right)^{-1} B_{aug}^T P_\infty \right) A_{aug} + \gamma^2 \left(\overline{Q} - P_\infty \right) = 0.$$

Providing a sufficiently large optimization horizon, N, the above modification ensures that[2]

$$\left|\left| X_\beta(k+j|k) \right|\right| \leq \gamma^j \left|\left| X_\beta(k) \right|\right|, \forall j \geq N_0. \tag{19}$$

From a linear algebraic point of view, the eigenvalues of the closed-loop system lie inside the circle $|z| \leq \gamma$ on the complex plane.[7]

2.6 | Recursive least squares (RLS) disturbance estimation

In the framework of DRC, in order to improve the overall robustness of the AVC system, we use an RLS estimator to reduce the power of the disturbance signal that affects the repetitive MPC. Based on discrete-time state Equation (1), the following regression model is considered for disturbance estimation:

$$\widehat{x}(k+1) - A\widehat{x}(k) - Bu(k) = Hd(k). \tag{20}$$

Here, $\widehat{x}(.)$ is obtained by imposing the inverse operator $\Gamma^{-1}(q^{-1})$ on the estimated state vector of the Kalman filter, $\widehat{X}(.)$. The RLS algorithm and a detailed discussion of its convergence/robustness properties can be found in Simon.[37] To achieve a 2-norm attenuation of the disturbance, the output of the RLS is fed-forwarded by the gain $(B^TB)^{-1}B^TH$ through the control channel (see Figure 2). The effectiveness of the RLS disturbance estimator in improving the robustness of the repetitive MPC will be confirmed by the experimental results at Section 4.

3 | EXPERIMENTAL APPARATUS AND THE REDUCED-ORDER PLANT

In this section, the experimental rigs that are used to obtain the reduced-order nominal plant for control design purposes, experimental modal analysis, and finally monitoring of the performance of the closed-loop system in real time are introduced. The plant is a vibrating clamped-free smart aluminum beam with the geometrical dimension, 440 × 40 × 3 mm. The host structure is assumed to be isotropic with Young's modulus 70 Gpa and density 2.7 g/cm^3. Two piezoelectric patches (DuraActTM P-876.A15) are attached on one side of the beam acting as the actuation elements. The optimality of the actuation power in controlling the mode shapes of the continuous structure is guaranteed by placing the piezo-patches according to robust-optimal actuator placement criterion that has been presented at Nestorović and Trajkov[48] The "optimal placement" terminology is based on the technique of balanced model reduction. The resulting system benefits equally from controllable and observable retained modes. Additionally, the algorithm in Nestorović and Trajkov[48] relies on the assortment of the modes based on their simultaneous controllability/observability Gramians. The optimality is guaranteed over H_2 and H_∞ norms of the transfer matrices of all placement candidates on the surface of the beam. As a result, the algorithm guarantees the globality of solution of sensor/actuator placement by evaluating all possible configuration. It should be pointed out that the noncollocated optimal structural configuration proposed in Nestorović and Trajkov.[48] introduces a time delay between the actuator and sensor elements which may be significant in large structures.[49] Unsurprisingly, a PD compensator may lead to instability while the delay increases due to real zeros on the right-hand side of the imaginary axis.

Two physical loops are involved in the implementation phase of modeling and control systems as, Figure 1a,b. Figure 1a, shown as Loop 1, presents the control execution circuit together with an external mechanical shaker. However, Figure 1b, which is indicated by Loop 2, is used for obtaining the internal model of disturbance, Equation (2), and later for evaluation of the closed-loop system in frequency-domain. It should be mentioned that in the last part of the experimental test both of the Loops 1 and 2 are activated simultaneously to compare the frequency response function (FRF) of the controlled system with the open-loop one. According to Oveisi and Nestorovic,[50] as shown in Figure 1a, the first piezo-patch is at 20 mm distance from the clamped end and the second patch stands in 80 mm from the first one. The velocity and the external excitation are measured through the corresponding measurement channels of the

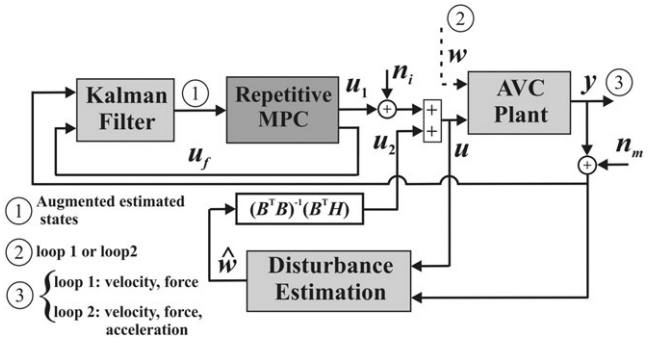

FIGURE 2 Schematic configuration of control system. AVC = active vibration control; MPC = model predictive control

acquisition system, connected to the laser vibrometer VH-1000-D, and the force sensor B&K Type 8230-001,[51,52] respectively. The digital laser Doppler vibrometer supplies the signal to the feedback channel of the control system. The force transducer provides the input measurement data for modal analysis. Because the free end of the beam is in oscillation and plays a significant role in the overall response of the system, the scanning digital laser is placed at the free end at 238 mm distance from the beam in its rest mode.

A mismatched disturbance is considered to be affecting the system behavior through an independent channel of the control input. For this purpose, a vibration exciter (Brüel&Kjær shaker Type 4809) is employed as the source of simulated disruption. The real-time analyses are carried out using dSPACE system with digital data acquisition (DAQ) DS1005 PPC Board with the working range of ± 10 V. The front end of the DAQ system consists an analog to digital converter (dSPACE ADC DS2004) and a digital to analog converter (dSPACE DAC DS2102). An amplifier (PI E-500) is utilized to amplify the generated signal by DAQ with a constant gain of 100 before sending it to the actuators. Similarly, another power amplifier (B&K Type 2706) is operated to amplify the signal generated by the dSPACE board for the vibration exciter (shaker in Figure 1a). The use of Brüel&Kjær 2706 amplifier separates the Loop 1 (control loop) from Loop 2 (experimental modal analysis). Accordingly, Loop 2 is activated by the third power amplifier (Brüel&Kjær amplifier Type 2718) with maximum output current of 1.8 A. The experimental modal analyses in Loop 2 are conducted on a LAN-XI DAQ Hardware (Brüel&Kjær Type 3160) with input/output of maximum 51.2 kHz direct current (DC) channels. The first input, as mentioned before, is the force transducer and the second input is 1D Piezoelectric CCLD accelerometer (Brüel&Kjær Type 4507) with the sensitivity of 100 mV/g which is collocated with the force sensor (see Figure 1b).

It should be mentioned that the piezo-elements are activated in the range of $[-200\ 200]$ V. Both of the controller and estimator systems are created on SIMULINK platform, and then the model is compiled and uploaded to the DAQ system in real time (see Figures 1a). Also, for experimental modal analyses PULSE, LabShop software is employed.

The prediction of the controller's trajectory in MPC framework as a model-based technique widely depends on the minimal formulation of the plant dynamics. The interconnection of the proposed repetitive MPC with the real-time plant is schematically shown in Figure 2. In this figure, w represents the disturbance realization on the control loop and the input data for the fast Fourier transformation (FFT) which is used to calculate the FRF of the plant from disturbance channel to output (acceleration). In the context of AVC, mostly the reduced-order model of the real plant is a linearization of the system around a single operating point. It should be mentioned that the identification is carried out by neglecting the torsional and in-plain modes of the beam. The underlying linear model is obtained through the two-step paradigm in frequency-domain system identification framework. The procedure starts with a nonparametric modeling of the system. For this purpose, the multireference modal analysis is carried out in the frequency ranges of interest which are [0 250] Hz for the lumped state space model and [0 800] Hz for the autonomous disturbance model. Next, the obtained FRFs are parameterized using frequency-domain subspace system identification method proposed in McKelvey, Akcay, and Ljung.[53] In order to manifest the identification quality, the response of the real structure is compared with the identified model in the nominal frequency range of Figure 3.

As it is depicted in Figure 3, an acceptable agreement exists between the system and the identified model. The state matrix is transformed into modal form, following the method proposed in Gawronski,[54] to assist the quantification of the weighting matrices later in designing procedure of the controller and Kalman gain. As a result, the interpretation of the states and output matrices can be explained in terms of physical variables such as modal velocity and modal displacement. On the other hand, it should be also noted that the employed subspace method, that is, McKelvey, Akcay, and Ljung[53] is a black-box scheme and as a result, it may include superficial states without physical interpretation. In order to address this problem, the order of the lumped model is kept at six considering the fact that there exist three natural frequencies in the working range. This selection results in sacrificing accuracy for having a better match between the nonparametric model and parametric one (compare FRFs in sub-Figures 3). This mismatch is due to (a) Neglecting the contribution of higher order dynamics to the frequency range of operation. (b) Neglecting the small time delay in input/output transfer matrix. (c) 80 dB difference between the resonance and antiresonance amplitudes which makes it difficult to correctly capture both by the algorithm. For the sake of briefness, further details are referred to the impressive contribution of Pintelon and Schoukens.[55] The obtained reduced order system as the nominal plant for controller design and disturbance estimation is discretized using abundantly small sampling time (500 μs). The sampling time is related to the maximum operational frequency of the plant and cannot be too small because it may be practically impossible to handle the computational efforts for each time increment. The nominal reduced-order system matrices are given in Appendix A.

Next, in order to extract the disturbance dynamics (Equation (2)) independent of the reduced-order model, an experimental modal analysis is performed by means of a shaker test in PULSE LabShop software.[32] Effective prediction of the control action mostly depends on the accuracy of the nominal model as well as the profile of the future disturbances. Accordingly, the shaker is attached to one end of the beam through a rubber band. Similarly, the accelerometer is collocated with the force sensor as shown in Figure 1b. While the piezo-actuators are inactive, the

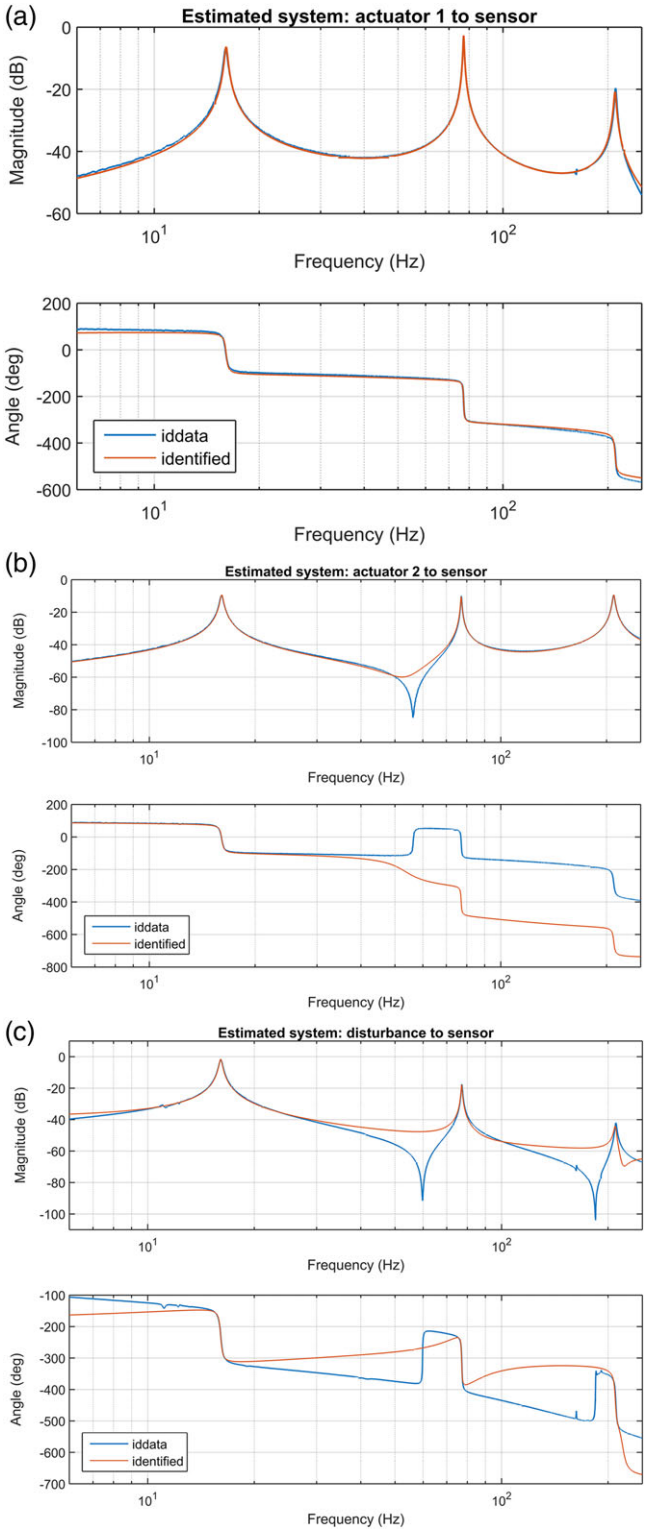

FIGURE 3 Frequency response of the real structure compared with the reduced-order system (output: LDV): (a) input: Actuator 1, (b) input: Actuator 2, (c) input: shaker

disturbance channel is triggered by a random signal in the frequency range of [0 800] Hz. A low-pass filter is considered to filter out the high frequency response of the transducer data before applying the FFT. Meanwhile, due to the nature of this excitation signal, leakage is a practical concern that leads to distortion of the measured FRF. To condense the leakage effect and simultaneously to keep the signal-to-noise ratio high, averaging with Hann window is employed. Subsequently, the FFT parameters such as the frequency range (sampling time of B&K 3160: 488.3 μs) is considered as a broad range of 6,400 lines (df = 125 mHz). The baseband analysis is carried out with 60 averages and 66.67% overlap. A 12th order the LTI object is adjusted to the obtained FRF to parameterize the autonomous exogenous system with a limited number of states in the augmented system of Equation (8). The FRF of the identified model is examined over the FRF of the experimental system in Figure 4. The state matrix of the disturbance model is given in Appendix A.

As one can see, the disturbance model is in a good agreement with the FRF of the actual structure. The quality of the measurement for identifying the internal model can be assessed by the coherence diagram in the nominal frequency range. Accordingly, as shown in Figure 5, the measurements have coherence closeness to one which indicates the linearity of the system response and the excitation. The low frequency-resolution of the measurement around the resonance and antiresonance states can be improved by using zoom analysis and increasing the number of FFT points which are not necessary for the scope of this paper.

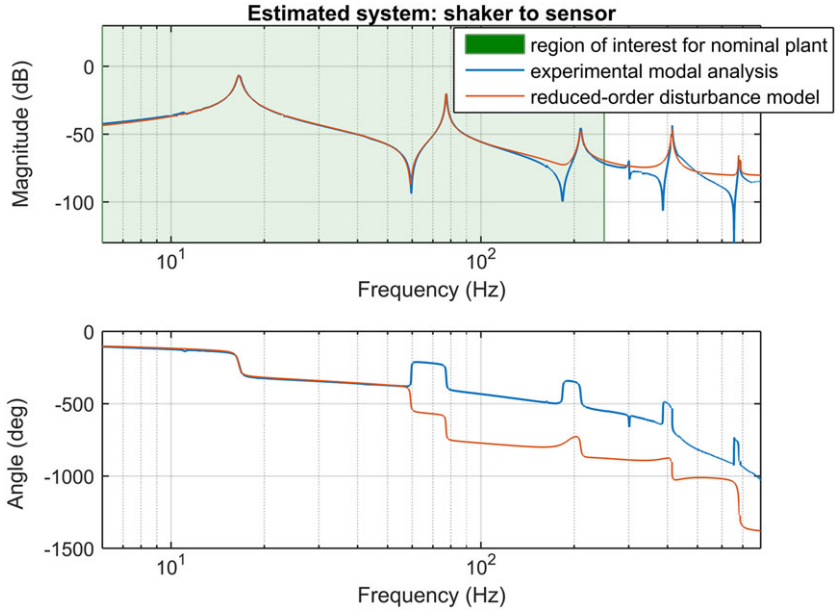

FIGURE 4 Frequency response function of the real structure relative to the 12th disturbance model

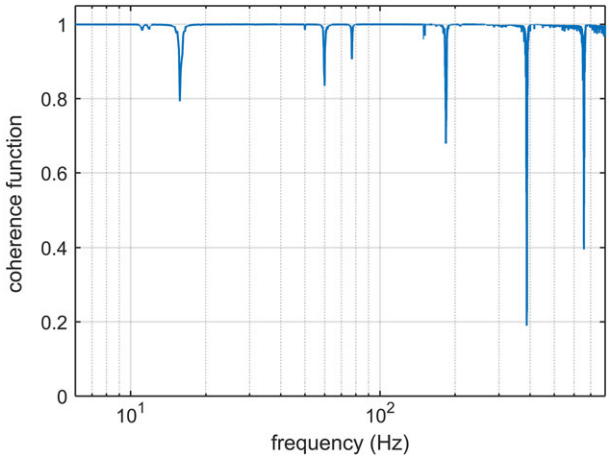

FIGURE 5 Frequency analysis of the coherence function for the disturbance model

4 | EXPERIMENTAL IMPLEMENTATION[1]

The robustness of the augmented AVC system in Equation (6) concerning the bounded parametric uncertainties is achieved as follows: In AVC of the mechanical structures with light damping ratios, the 2-norm bound of the perturbations due to unknown variations and noises is much lower in magnitude compared with the nominal gains of the system in the respective frequencies. Therefore, assuming the vibrations remain in the linear region and the excitation frequency is limited to the range that the disturbance model is valid, due to the IMP, the perturbations will be rejected asymptotically by the asserted control arrangements. The control input noise (n_i; see Figure 2), as well as the measurement noise (n_m; see Figure 2) are assumed bounded disturbances modeled as white noise signals with normal distributions. Thereby, the use of Kalman filter as the estimator is justified. With computation demand being one of the primary sources of practical limitations, reducing excessive overhead for online implementations is achieved by calculating and storing the gain matrix $K_f(.)$, offline.

In the rest of this section, the experimental results are presented for the implementation of proposed controller on the piezo-laminated beam shown in Figure 1a,b. The higher mode shapes of the structure that lie out of the nominal frequency range are considered as the source of uncertainty and should not be activated unless the disturbance is focused on this area. The spillover rejection is examined in detail in the last part of the experimental results. In the run-time phase of implementation, the following tasks are carried out sequentially:

At each sampling instant (k), the future trajectory of the plant state vector is predicted over the optimization horizon N under the action of the predicted control trajectory. The predicted control trajectory along the optimization horizon is parameterized by a suitable Laguerre network. The predictive controller determines the Laguerre parameterization variables by solving an open-loop optimal control problem entailing the output regulation objectives. By the receding horizon policy, only the first component of the obtained optimal solution is applied and then, the overall process repeated in the next sampling instant, $k + 1$. The tuning factors of the MPC system are the optimization horizon N, the weighting matrices Q and R, the data weighting parameter β, the prescribed degree of stability γ and the scale factors a_i, and dimensions N_i of the parametrization Laguerre networks. This section discusses the tuning process of the control system; the keywords "Online" and "Offline" in the beginning of each step indicate the state at which the procedure is carried out.

- Offline: The augmented model is constructed having the state space matrices A, B, H, and C, K_f as the observation gain, prediction horizon, the weighting matrices in optimal control design, and matrices S, E in Equation (2).
- Offline: Considering the MPC weight matrices, we use $Q = 10C_{aug}^{T}C_{aug}$ to minimize the output error and $R = 3 \times 10^{-3}I_2$ (I_n is the $n \times n$ identity matrix) to achieve a fast transient response. To guarantee the stability, the desired disk for the closed-loop eigenvalues is specified by $\gamma = 0.95$. The LQR problem associated with these parameters is considered as the reference LQ performance. The data weighting is selected by $\beta = 2.1$ to remedy the numerical ill-condition issue of the MPC optimization problem.
- Offline: The optimization horizon N should be selected according to the AVC frequency range. Generally, faster dynamic systems require larger optimization horizons to achieve stability and optimality. To examine this criterion numerically, for each N, we compare the closed-loop eigenvalues of the unconstrained MPC (11) with those of the LQR. By this method, $N = 20$ produces a satisfactory LQ performance.
- Offline: The scale factors $a_1 = 0.76$ and $a_2 = 0.76$ of the parameterization Laguerre functions are selected to be close to the dominant closed-loop eigenvalues of the LQR.[2] Setting $N = 20$, we gradually increase the number of the Laguerre functions so that the closed-loop eigenvalues of the unconstrained parameterized MPC (17), converge to those of the LQR. Using a trial and error procedure, we select $N_1 = 5$ and $N_2 = 5$ to achieve an acceptable performance.
- Offline: The Kalman filter gain is calculated to estimate the augmented state vector, and then it is stored in the memory. Regarding the stationary initial state of the system, the estimation covariance is initialized by a small value $P_{f0} = 10^{-4}I_8$. Referring to the data sheet of highly accurate LDV,[51] a nominal value for the measurement noise covariance is considered. Owing to the internal model property of the operator $\Gamma(q^{-1})$, the disturbance signal $d(.)$ is eliminated from the augmented system (6). Accordingly, from a practical Kalman filtering viewpoint, Q_f is conceived as the covariance of two noise components: (a) a noise acting through the control channel due to the force transducers; (b) a fictitious noise accounting for the unmodeled/remainder perturbations. Therefore,

[1]Interested reader may contact the corresponding author to receive the implementation .mdl SIMULINK files as well as the designing scripts in MATLAB.

$Q_f = B_{aug} Q_u B_{aug}^{\mathrm{T}} + Q_{fic}$, where Q_u is the covariance of force transducer noise (obtained from the data sheet[52]) and Q_{fic} is the fictitious noise covariance which also makes Q_f nonsingular. To guarantee both stability and optimality of the Kalman filter, an iterative tuning procedure is applied as follows. Starting from the nominal covariance matrices, the eigenvalues of the steady state filter, that is, $\mathrm{eig}(A_{aug} - K_f(k) C_{aug})$ for large k, are compared with those of the corresponding LQR observer. Following this method, the covariance matrices are finely tuned as: $Q_f = 4.9{\times}10^{-9} B_{aug} B_{aug}^{T} + 10^{-9} I_8, R_f = 2{\times}10^{-4}$.

- Offline: The general interconnection of the state-observer and disturbance estimator are realized in SIMULINK based on Figures 1a and 2.
- Offline: Then, the model from SIMULINK is built and a C++ code for dSPACE module is generated.
- Online: Using the estimated state vector $\widehat{X}(.)$, the optimization problem (17) is solved by a suitable QP solver under the control saturation constraint. Subsequently, the optimal Laguerre parameterization is calculated and the current control action is obtained.
- Online: The analog input data from plant's output (Laser Doppler vibrometer) as well as the force transducer are read accordingly.
- Online: The states are reconstructed from the augmented observer and the disturbance is estimated.
- Online: Retrieving the control input generated by QP and writing the outcome in input/output board to be converted to analog form, amplified, and applied on the active piezo-actuators are automatically performed next.
- Offline: All the required variables are saved to be presented using ControlDesk in a limited time-window.

In the simulations, to carry out the optimization involved in the predictive control formulation, a fast QP solver known as Hildreth's algorithm is employed.[7] A notable advantage of this algorithm is its ability to recover a suboptimal solution in the case of conflicting constraints.

After constructing the control system based on Equations (17) and (18) in SIMULINK and compiling it to dSPACE RTI platform, the system is excited through the disturbance channel with a pulse period equal to 5 s which is active for 2.5 s (50%). The uncontrolled and controlled systems are realized on the real-time DAQ of the dSPACE with the sampling frequency of 500 MHz. The captured velocity from the laser vibrometer for three cases of controlled (MPC), controlled (PID), and uncontrolled systems are compared in Figure 6. The choice of PID is due to the fact that it is pertinent to implement PD and PID as a widely accepted technique in industry. Additionally, as pointed out in Koerber and King and Dang et al.[56,57] the effective use of information on actuator constraints and behavioral prediction can avoid performance violations that are commonly happening in alternative techniques in real-time applications. The PID controllers are tuned on each of the input channels separately. It can be seen that the performance of the PID controller even around the fundamental natural frequency cannot match the repetitive MPC controller. Moreover, the PID-based closed-loop system is unable to reject the disturbance of high-frequency nature as it is shown in the later frequency analysis.

Remark 3. Comparing two independent control strategies is a critical matter because an analogy does not exist for tuning the two. In other words, in applied control problems, one method can be tuned better than

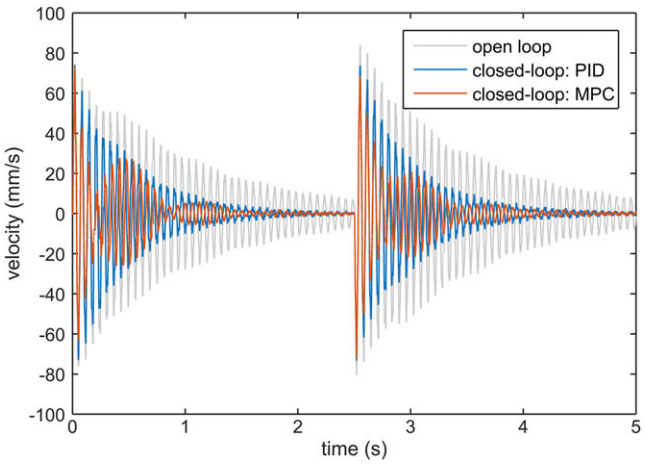

FIGURE 6 Disturbance rejection performance of the closed-loop system based on repetitive model predictive control (MPC) and PID

the other. Nonetheless, in this research, a fair comparison is obtained by first tuning the PID controller to its best and then trying to match the same control level with repetitive MPC. However, better performances may be achieved by tuning MPC or including higher order mode-shapes in the model of the reduced system for which the MPC will perform significantly better. Because the order of the PID as a model-free controller is limited, authors tried to limit the model order for a fair comparison. Additionally, comparison of MPC with LQR has been tackled in the remarkable work of Bossi et al.[10] Later in this paper for the case, where the hard constraints are activated (here: actuator saturation), the enactment of the anticipated control system is compared with the LQG controller.

The control efforts on both the piezo-actuators are depicted in Figure 7 for two closed-loop systems. The applied control signals on piezo-actuators are in the acceptable range of [−200 200] V with smooth variations. It is worth mentioning that, any disturbance signal with an abrupt change in amplitude such as pulse-type signals may excite the high-order dynamics of the system which are not included in control development procedure.

The output estimation error based on Kalman filter is presented in Figure 8 which indicates the effectiveness of the state estimation system.

In order to distinguish between the repetitive MPC and the repetitive MPC together with feedforward disturbance rejection system, a chirp signal is realized in the disturbance channel. The frequency of the excitation is developed from 1 to 250 Hz in four cases of the open-loop and closed-loop systems: (a) repetitive MPC, (b) repetitive MPC together with

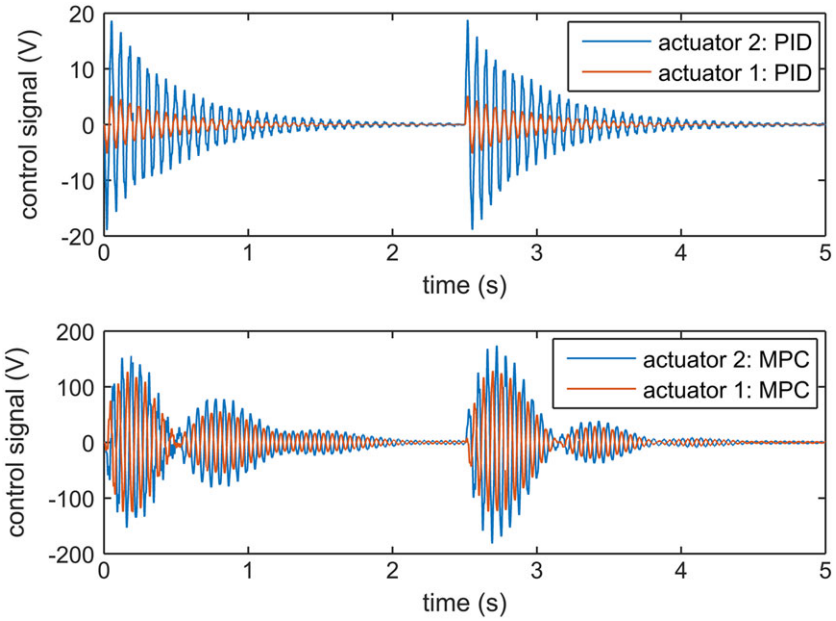

FIGURE 7 Applied control efforts on piezo-actuators. MPC = model predictive control

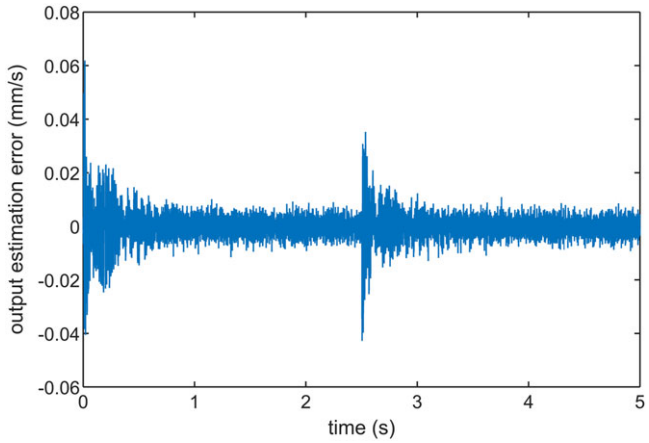

FIGURE 8 Observation error for the plant output

disturbance estimation/rejection system, and (c) PID compensator. The responses of the plant for the controlled and uncontrolled cases are shown in Figure 9 in the time-domain based on the measurement signal generated from Doppler vibrometer, which is further fed to the dSPACE ADC board (DS2004).

Figure 9 displays a comprehensive evaluation of the vibration attenuation routine in the nominal frequency range. It can be observed that the MPC controller design, based on the reduced order identified model, suppressed the vibration magnitude within the considered frequency range. A distinct advantage of the repetitive MPC based on the modal realization of the reduced-order model is the possibility of defining frequency-dependent (mode-dependent) weighting matrices that designate an emphasis on a restricted frequency range. The advantage of the repetitive MPC to the PID is revealed in the higher frequencies where substantial suppression can be achieved by MPC compared to PID. Additionally, the MPC based on the disturbance estimation has a better performance in attenuating the vibration amplitude. The corresponding control efforts that are generated for piezo-modules by the dSPACE DAC board are shown in Figure 10.

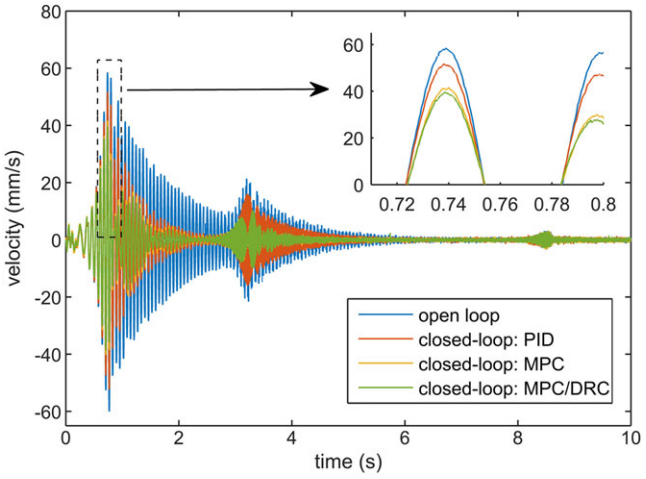

FIGURE 9 Experimental comparison of measured outputs in time-domain for chirp excitation. DRC = disturbance rejection control; MPC = model predictive control

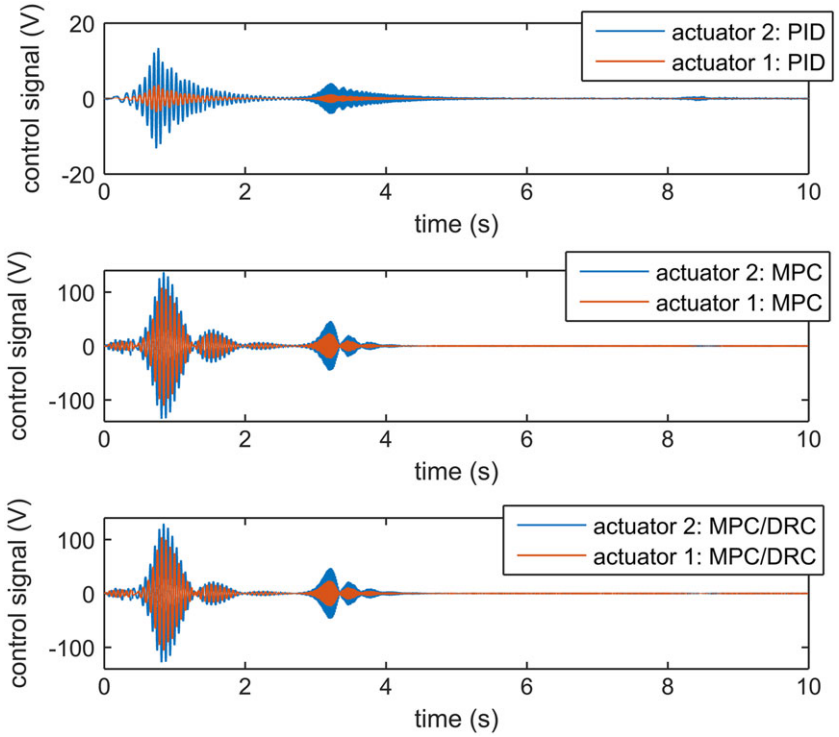

FIGURE 10 Control effort applied on the piezo patch actuators. DRC = disturbance rejection control; MPC = model predictive control

Figure 10 shows that the control efforts implemented to each of the piezo-actuators are restricted to maximum 140 V with a smooth behavior. The experimental determinations confirm that the regulator system functions properly in attenuating the vibration amplitude in the presence of structured uncertainties in system elements. Also, the estimation error of the velocimeter is represented in Figure 11.

Next, the performance of the control system is evaluated in the frequency-domain. For this purpose, loop 1 (the control loop) in Figure 1a is activated while the shaker is attached to loop 2 (the modal analysis loop). The generator is triggered by PULSE with a random signal in the range of [0 800] Hz. In order to assess the spillover effect, the cut-off frequency of the low-pass filter in the force transducer measurement channel is set to 800 Hz. As a result, based on FFT, the sampling time is calculated as 488.3 μs, and the number of lines is selected to be 6400 (sampling frequency of 125 mHz) to prevent long experimental duration. In order to address the leakage error and similarly to the case of disturbance dynamics, averaging with Hann-window is engaged. Accordingly, a baseband analysis is carried out with 20 averages and 66.67% overlap for an overall duration of ≈60 s. The experimental configurations in the described form are examined by the same parameters four times: open-loop (loop 1 is deactivated), closed-loop based on repetitive MPC, closed-loop based on repetitive MPC disturbance estimation/rejection, and closed-loop based on PID controller. The FRF of the system, as well as the phase diagram, are shown in Figure 12.

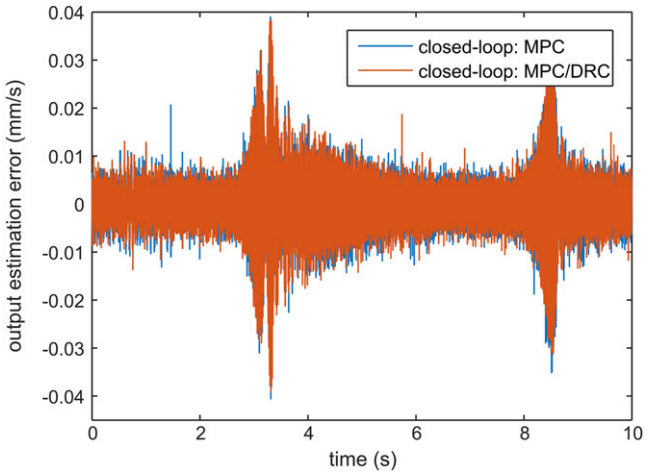

FIGURE 11 Estimation error of the output based on Kalman filter. DRC = disturbance rejection control; MPC = model predictive control

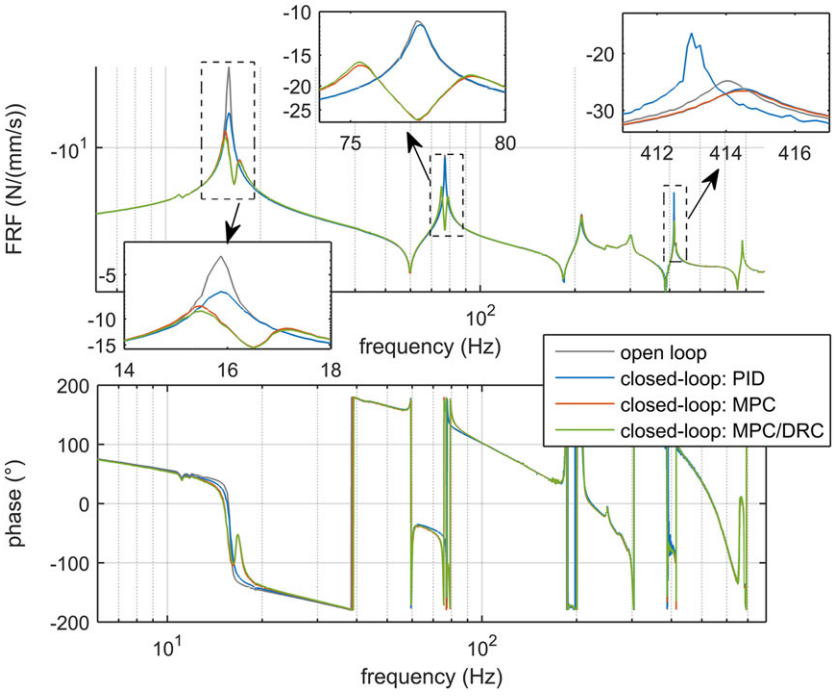

FIGURE 12 Frequency domain analysis of the closed-loop systems for vibration attenuation performance evaluation. DRC = disturbance rejection control; MPC = model predictive control

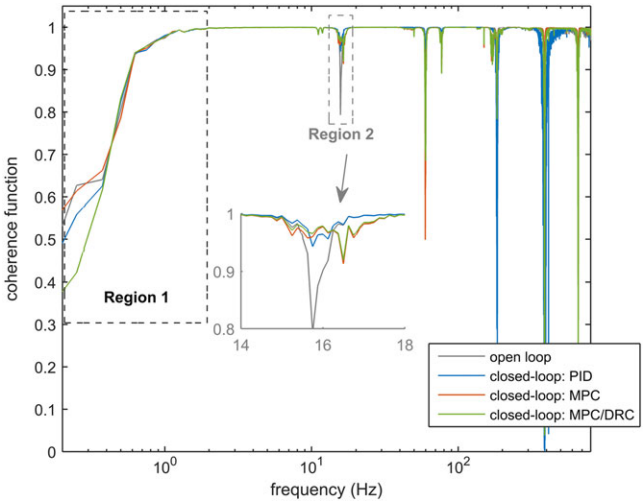

FIGURE 13 Coherence diagram for experimental modal analysis of the closed-loop systems. DRC = disturbance rejection control; MPC = model predictive control

The first observation is that although the PID controller had an acceptable performance in Figure 6, it is unable to control any higher mode-shape of the structure without additional tuning of the parameters. For instance, in contrast to both of the methods based on the MPC idea, the second mode shape of the system is undamped employing PID regulator. Moreover, at high frequencies such as in the range of [411 417] Hz, the performance of the closed-loop system based on the PID compensator is even worth than the open-loop uncontrolled case. The second observation is the high vibration attenuation factor for both the repetitive MPCs even at frequencies where the nominal plant model is not valid. This emphasizes the importance of incorporating a broadband disturbance model based on IMP in control synthesis. Then, it can be observed that in the nominal frequency range of reduced order plant, the MPC based on estimated disturbance a higher suppression level compared to repetitive MPC.

Since the quality of the FFT is the crucial parameter that validates the FRF obtained based on experimental modal analysis, the coherence of the measurements is presented in Figure 13. The coherence function is used as a data quality assessment tool which identifies how much of the output signal is related to the measured input signal. The coherence equal to 1 denotes the perfect measurement. Based on Figure 13, three regions are less reliable analyses:

1. Frequencies below 6 Hz: This is the frequency range which shaker is practically unable to excite. Since the structure under study does not have any resonant frequencies in this range, the deterioration of the result below 6 Hz may be neglected.
2. Around the first natural frequency and other resonance and anti-resonance frequencies: This case is a typical behavior of the system in baseband analysis. In order to improve the measurement results, a solution may be a zoom analysis which mostly used when the modal parameters such as natural frequencies and damping ratios of the system are the primary concern. Since in this paper, the focus is lighted on vibration control this step is relinquished. It is observed in the subplot of coherence diagram between 14 and 18 Hz that due to a significant reduction of vibration amplitude in the resonance state of the structure, the coherence of the closed-loop systems based on MPC is close to one. In contrast to MPC, the PID controller though reducing the vibration amplitude, changes the resonance state and thereby needs to be taken care of in new resonant modes. This emphasizes the advantage of MPC from another point of view.

A notable advantage of the repetitive MPC is the spillover rejection when the excitation is in the nominal frequency range of the reduced-order model. In other words, the controller can reject the disturbances of high-order dynamics. With a view to present this quality, FFT analysis (H_2 function in[58]) is performed to obtain an estimation of FRF of the control system in an attempt to identify the dominant frequencies of the controller Figure 14. The first observation is that the two primary actuation authorities on the nominal mode shapes of the reduced-order system are on two fundamental natural frequencies. This feature ensures that the control system has captured the key influential mode shapes

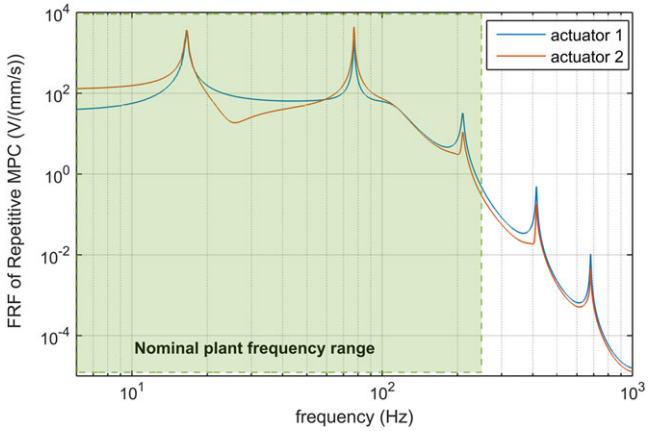

FIGURE 14 Frequency response function (FRF) of the control system in the nominal frequency range of the internal model

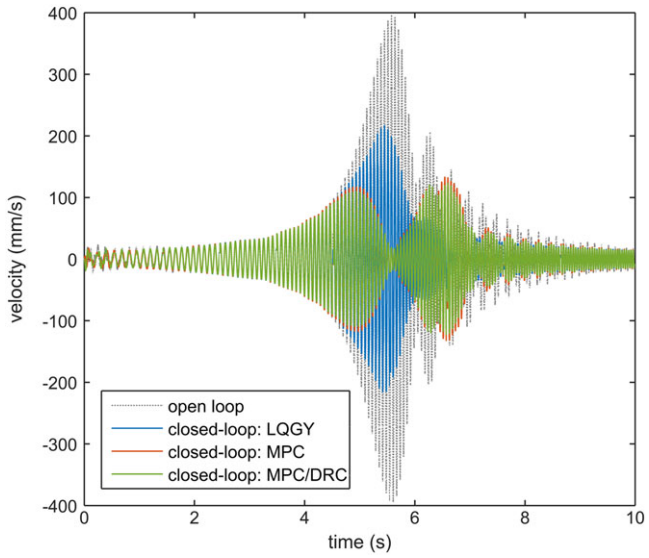

FIGURE 15 Transient behavior of the open-loop system compared with the controlled ones in the saturation incident. DRC = disturbance rejection control; MPC = model predictive control

of the system correctly. Moreover, although the controller can prevent spillover effect due to the slope of FRF at high frequencies, it can still attenuate the higher order unmodeled dynamics within the frequency range of the internal model. The latter is a promising feature especially when the order of the controller is limited because of the processing hardware limitations.

Finally, by aiming at evaluating the proposed closed-loop configuration in the saturation event, an LQG controller for output regulation problem is designed. For this purpose, a steady state Kalman filter is combined with a standard LQRY, and then the design matrices are tuned to achieve a high attenuation level.[2] In the experimental simulations, the disturbance level is increased intentionally such that the control signals stand higher than the saturation level (200 V in magnitude). Final tunings of the LQGY are carried out such that the control systems under comparison experience the same amount of time in saturation which is essential for a fair assessment. Because the LQGY is unable to handle such hard constraints on the control input, a saturation block added to the SIMULINK model before compiling it into C language and uploading the compiled file to DS 1005 PPC board. Then, the three control systems are evaluated in real time for a mismatch chirp disturbance signal which is active for 10 s covering the frequency range of [6 25] Hz. The transient responses of the open-loop system against three closed-loop ones are shown in Figure 15. It can be seen that MPC-based methods achieved higher attenuation while satisfying the hard constraints. Moreover, the applied control signals on the piezo-actuators are depicted respectively in subplots of Figure 16.

[2]Use `kalman` and `lqry` functions sequentially in MATLAB to design the LQG output regulator.

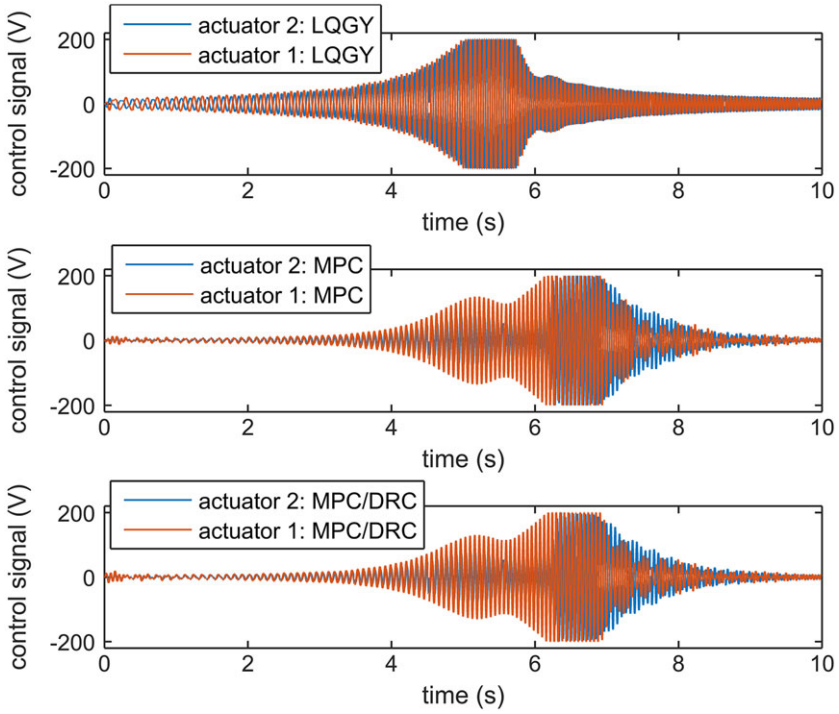

FIGURE 16 Constrained control signals of the MPC-based methods compared with LQGY regulator. DRC = disturbance rejection control; MPC = model predictive control

5 | CONCLUSION

In this paper, an observer-based MPC method is proposed for disturbance rejection control. The feedback control process is developed in the framework of a repetitive MPC, and a recursive least squares algorithm is utilized for disturbance estimation/rejection. To put in a nutshell, the main contributions of the control system developed in this paper are the following:

- The internal model-based repetitive control paradigm provides an efficient framework for rejecting periodic disturbances in AVC systems. This approach can be conceived as the generalization of the classic integral action used in PID controllers. The integral action, however, rejects only step-type disturbances with zero steady state error. Moreover, incorporating an internal model of the disturbance signals guarantees asymptotic rejection of the disturbances. Conventional approaches to robustify MPC systems against disturbances, such as min-max optimization,[46] are computationally demanding and then achieve only disturbance attenuation rather than disturbance rejection. In this respect, internal model-based MPC is prominent in terms of both robustness and computational efficiency.
- In comparison with the conventional industrial control techniques, such as PID, a remarkable feature of the MPC is its ability to handle hard system constraints and nonlinearities such as actuator saturation. Explicit formulation of the limitations in MPC guarantees the stability under nonlinear effects as well as an optimal closed-loop performance.
- In comparison with the common MPC algorithms, parameterization of the control inputs by orthonormal basis functions considerably reduces the computational burden of the associated numerical optimization. For example, in the AVC application reported in this paper, Laguerre parameterization resulted in a 75% reduction in the number of the optimization variables with respect to the conventional MPC algorithm. Accordingly, fast optimization solvers can be used to benefit from the MPC advantages in AVC systems.
- The over-specification of the controller's output by augmenting a soft saturation element before submitting the control law to the actuator of AVC in morphing structures is undesirable. This eventually excites the unmodeled dynamics of high order nature that are not included in the nominal model of the plant. Similar observations are reported in Peng et al. and Sun and Mills.[59,60] This observation is verified by comparing the performance of the proposed control algorithms to the LQG output regulation technique.
- For geometrically linear vibration amplitudes and for the disturbance frequencies limited to the range in which the internal model is valid, the perturbations are guaranteed to be asymptotically rejected. This perception is observed in time- and frequency-domain results of the experimental implementations.

- By simulating the bounded disturbance signal with abrupt jumps in amplitude, the performance of the control system is proven to be robust against the high-order unmodeled dynamics of the system. Additionally, as a notable behavior, the repetitive MPC shows the capability to cut off the spillover effect of the actuators in the nominal frequency range of the reduced-order model.

ORCID

Atta Oveisi http://orcid.org/0000-0002-6507-9448
Mehran Hosseini-Pishrobat http://orcid.org/0000-0002-5866-5131
Tamara Nestorović http://orcid.org/0000-0003-0316-2171
Jafar Keighobadi http://orcid.org/0000-0002-1216-4518

REFERENCES

[1] T. Sardarmehni, J. Keighobadi, M. B. Menhaj, H. Rahmani, *Archives Civil Mech. Eng.* **2013**, *13*(4), 432. https://doi.org/10.1016/j.acme.2013.05.003

[2] L. Wang. *Model Predictive Control System Design and Implementation Using MATLAB®*. London: Springer London; **2009**. https://doi.org/10.1007/978-1-84882-331-0.

[3] L. C. Henriksen. Information and Mathematical Modeling, Technical University of Denmark, Lyngby, **2007**.

[4] W. H. Lio, J. A. Rossiter, B. L. Jones. 2014 *UKACC International Conference on Control (CONTROL)*, IEEE; **2014**. https://doi.org/10.1109/CONTROL.2014.6915220.

[5] P. Boscariol, A. Gasparetto, V. Zanotto, *J. Intell. Robot. Syst.* **2010**, *58*(2), 125. https://doi.org/10.1007/s10846-009-9347-5

[6] G. Gibbs, S. S. Canada, *Acta Astronaut.* **2002**, *51*(1–9), 591. https://doi.org/10.1016/S0094-5765(02)00077-2

[7] L. Wang, C. T. Freeman, S. Chai, E. Rogers, *J. Process Control* **2013**, *23*(7), 956. https://doi.org/10.1016/j.jprocont.2013.03.012

[8] J. Friis, E. Nielsen, J. Bonding, F. D. Adegas, J. Stoustrup, P. F. Odgaard. *IEEE Conference on Decision and Control and European Control Conference*, IEEE; **2011**. https://doi.org/10.1109/CDC.2011.6160948.

[9] M. Benosman, G. Le Vey, *Robotica* **2004**, *22*(5), 533. https://doi.org/10.1017/S0263574703005642

[10] L. Bossi, C. Rottenbacher, G. Mimmi, L. Magni, *Control. Eng. Pract.* **2011**, *19*(10), 1087. https://doi.org/10.1016/j.conengprac.2011.05.003

[11] S. M. Hasheminejad, A. Oveisi, *Int. J. Mech. Mater. Des.* **2016**, *12*(1), 1. https://doi.org/10.1007/s10999-015-9293-2

[12] S. Li, J. Li, Y. Mo, *IEEE Trans. Ind. Electron.* **2014**, *61*(12), 6892. https://doi.org/10.1109/TIE.2014.2317141

[13] A. Oveisi, T. Nestorović, *Mech. Syst. Signal Process.* **2016**, *76–77*, 58. https://doi.org/10.1016/j.ymssp.2016.01.015

[14] A. Oveisi, R. Shakeri, *Eng. Struct.* **2016**, *116*, 1. https://doi.org/10.1016/j.engstruct.2016.02.040

[15] T. Nestorović-Trajkov, U. Gabbert, *Struct. Control Health Monit.* **2006**, *13*(6), 1068. https://doi.org/10.1002/stc.94

[16] H. Du, J. Lam, K. Y. Sze, *J. Sound Vib.* **2004**, *273*(4), 1031. https://doi.org/10.1016/S0022-460X(03)00520-0

[17] H. Yazici, R. Guclu, I. B. Kucukdemiral, M. N. Alpaslan Parlakci, *J. Dyn. Sys., Meas., Control.* **2012**, *134*(3), 31013. https://doi.org/10.1115/1.4005500.

[18] M. Nezami, B. Gholami, *Smart Mater. Struct.* **2016**, *25*(3), 35043. https://doi.org/10.1088/0964-1726/25/3/035043

[19] M. Hassan, R. Dubay, C. Li, R. Wang, *Mechatronics* **2007**, *17*(6), 311. https://doi.org/10.1016/j.mechatronics.2007.02.004

[20] A. Oveisi, M. Gudarzi, *J. Low Frequency Noise Vibration Active Control* **2013**, *32*(1–2), 41. https://doi.org/10.1260/0263-0923.32.1-2.41

[21] E. Omidi, S. N. Mahmoodi, *J. Vib. Control.* **2016**, *22*(10), 2434. https://doi.org/10.1177/1077546314548471

[22] A. Oveisi, T. Nestorović, *Mech. Eng.* **2016**, *14*(1), 37.

[23] J. G. Njiri, D. Söffker, *Renew. Sust. Energ. Rev.* **2016**, *60*, 377. https://doi.org/10.1016/j.rser.2016.01.110

[24] E. F. Mulder, M. V. Kothare, M. Morari, *Automatica* **2001**, *37*(9), 1407. https://doi.org/10.1016/S0005-1098(01)00075-9

[25] G. Li, G. Herrmann, D. P. Stoten, J. Tu, M. C. Turner, *Int. J. Control.* **2011**, *84*(1), 123. https://doi.org/10.1080/00207179.2010.542774

[26] S. Galeani, S. Tarbouriech, M. Turner, L. Zaccarian, *Eur. J. Control.* **2009**, *15*(3–4), 418. https://doi.org/10.3166/ejc.15.418-440

[27] A. G. Wills, D. Bates, A. J. Fleming, B. Ninness, S. O. R. Moheimani, *IEEE Trans. Control Syst. Technol.* **2008**, *16*(1), 3. https://doi.org/10.1109/TCST.2007.903062

[28] J. M. Maciejowski, *Predictive Control with Constraints*, Prentice Hall, Edinburgh Gate, Harlow, Essex, CM20 2JE, England **2002**.

[29] S. J. Qin, T. A. Badgwell, *Control. Eng. Pract.* **2003**, *11*(7), 733. https://doi.org/10.1016/S0967-0661(02)00186-7

[30] G. Takács, B. Rohal'-Ilkiv, *J. Vib. Control.* **2014**, *20*(13), 2061. https://doi.org/10.1177/1077546313479993

[31] P. Boscariol, A. Gasparetto, V. Zanotto, *J. Dyn. Syst. Meas. Control.* **2010**, *132*(1), 14506. https://doi.org/10.1115/1.4000658

[32] R. Dubay, M. Hassan, C. Li, M. Charest, *ISA Trans.* **2014**, *53*(5), 1609. https://doi.org/10.1016/j.isatra.2014.05.023

[33] K. R. Muske, J. B. Rawlings, *AIChE J* **1993**, *39*(2), 262. https://doi.org/10.1002/aic.690390208

[34] M. Hosseini-Pishrobat, J. Keighobadi, *Proc. Inst. Mech. Eng. C J. Mech. Eng. Sci.* **2015**, *239*(17), 3055. https://doi.org/10.1177/0954406215607899

[35] A. Isidori, L. Marconi, A. Serrani. *Fundamentals of Internal-Model-Based Control theory*, Springer, London; **2003**. https://doi.org/10.1007/978-1-4471-0011-9_1.

[36] S. Hara, Y. Yamamoto, T. Omata, M. Nakano, *IEEE Trans. Autom. Control* **1988**, *33*(7), 659. https://doi.org/10.1109/9.1274

[37] D. Simon. *Optimal State Estimation: Kalman, H∞, and Nonlinear Approaches*. Hoboken, NJ, USA: John Wiley & Sons, Inc.; **2006**. https://doi.org/10.1002/0470045345.

[38] E. Lavretsky, K. A. Wise. Springer London; **2013**. https://doi.org/10.1007/978-1-4471-4396-3_3.

[39] J. A. Rossiter, B. Kouvaritakis, M. J. Rice, *Automatica* **1998**, *34*(1), 65. https://doi.org/10.1016/S0005-1098(97)00171-4

[40] B. Kouvaritakis, J. A. Rossiter, J. Schuurmans, *IEEE Trans. Autom. Control* **2000**, *45*(8), 1545. https://doi.org/10.1109/9.871769

[41] L. Wang. *Proceedings of the 40th IEEE Conference on Decision and Control (*Cat. *No.01CH37228)*, vol. 5, IEEE; **2001**. https://doi.org/10.1109/.2001.980976.

[42] A. Bemporad, M. Morari, V. Dua, E. N. Pistikopoulos, *Automatica* **2002**, *38*(1), 3. https://doi.org/10.1016/S0005-1098(01)00174-1

[43] M. M. Seron, G. C. Goodwin, J. A. de Doná, *Asian J. Control* **2003**, *5*(2), 271.

[44] P. Heuberger, P. Van den Hof, B. Wahlberg. *Modelling and Identification with Rational Orthogonal Basis Functions*. London: Springer London; **2005**. https://doi.org/10.1007/1-84628-178-4.

[45] D. Q. Mayne, J. B. Rawlings, C. V. Rao, P. O. M. Scokaert, *Automatica* **2000**, *36*(6), 789. https://doi.org/10.1016/S0005-1098(99)00214-9

[46] M. Ławryńczuk. Stability and Robustness of MPC Algorithms. *Computationally Efficient Model Predictive Control Algorithms, vol. 3*, Springer International Publishing, Cham, Switzerland **2014**. https://doi.org/10.1007/978-3-319-04229-9_7.

[47] J. A. Primbs, V. Nevistić, *Automatica* **2000**, *36*(7), 965. https://doi.org/10.1016/S0005-1098(00)00004-2

[48] T. Nestorović, M. Trajkov, *Mech. Syst. Signal Process.* **2013**, *36*(2), 271. https://doi.org/10.1016/j.ymssp.2012.12.008

[49] R. H. Cannon, E. Schmitz, *Int. J. Robotics Res.* **1984**, *3*(3), 62. https://doi.org/10.1177/027836498400300303

[50] A. Oveisi, T. Nestorovic, *J. Vib. Control.* **2016**: 1077546316651548. https://doi.org/10.1177/1077546316651548, 722.

[51] OMETRON User Manual, Portable Vibtrometer VH-1000-D. Harpenden, Hertfordshire, AL5 5BZ, UK: **2004**.

[52] Product Data: DeltaTron Force Transducers 8230-001. DK-2850 Nærum ·Denmark: **2017**.

[53] T. McKelvey, H. Akcay, L. Ljung, *IEEE Trans. Autom. Control* **1996**, *41*(7), 960. https://doi.org/10.1109/9.508900

[54] W. K. Gawronski, *Dynamics Control Struct.: A Modal Approach* **2004**. https://doi.org/10.1007/978-0-387-21855-7

[55] R. Pintelon (Rik), J. Schoukens (Johan). *System identification : a frequency domain approach*. Wiley; **2012**.

[56] A. Koerber, R. King, *IEEE Trans. Control Syst. Technol.* **2013**, *21*(4), 1117. https://doi.org/10.1109/TCST.2013.2260749

[57] D. Q. Dang, S. Wu, Y. Wang, W. Cai. *2010 Conference Proceedings IPEC*, IEEE; **2010**. https://doi.org/10.1109/IPECON.2010.5697119.

[58] P. Verboven, *Frequency-Domain System Identification for Modal Analysis*, Vrije Universiteit Brussel, Brussels **2002**.

[59] K. Peng, B. M. Chen, T. H. Lee, V. Venkataramanan, *Mechatronics* **2004**, *14*(9), 965. https://doi.org/10.1016/j.mechatronics.2004.06.002

[60] D. Sun, J. K. Mills. *Proceedings. 1998 IEEE/RSJ International Conference on Intelligent Robots and Systems. Innovations in Theory, Practice and Applications (Cat. No.98CH36190)*, vol. 1, IEEE; **1998**. https://doi.org/10.1109/IROS.1998.724695.

How to cite this article: Oveisi A, Hosseini-Pishrobat M, Nestorović T, Keighobadi J. Observer-based repetitive model predictive control in active vibration suppression. *Struct Control Health Monit*. 2018;e2149. https://doi.org/10.1002/stc.2149

APPENDIX A

The following state matrices are used as the reduced order identified system in state space form

$$
\begin{aligned}
A &= \begin{bmatrix}
-9.58 & 1.317E3 & 0 & 0 & 0 & 0 \\
-1.317E3 & -9.58 & 0 & 0 & 0 & 0 \\
0 & 0 & -1.68 & 484.65 & 0 & 0 \\
0 & 0 & -484.65 & -1.68 & 0 & 0 \\
0 & 0 & 0 & 0 & -0.95 & 101 \\
0 & 0 & 0 & 0 & -101 & -0.95
\end{bmatrix}, \\
B &= \begin{bmatrix}
-0.73 & 0.7 & 3.75 & -1.28 & 1.49 & -0.42 \\
3.30 & -1.68 & -1.04 & 0.68 & 1.04 & -0.36
\end{bmatrix}^{T}, \\
C &= \begin{bmatrix} -1.16 & 1.32 & -0.32 & 0.75 & 0.51 & -0.31 \end{bmatrix}, \\
H &= \begin{bmatrix} -0.05 & 0.06 & 0.23 & 0.46 & -2.54 & -0.84 \end{bmatrix}^{T}, \\
S &= \operatorname{diag}\left(\begin{bmatrix} -12.42 & 4.28E3 \\ -4.28E3 & -12.42 \end{bmatrix}, \begin{bmatrix} -8.88 & 2.6E3 \\ -2.6E3 & -8.88 \end{bmatrix}, \begin{bmatrix} -10.6 & 1.32E3 \\ -1.32E3 & -10.6 \end{bmatrix}, \right. \\
&\quad \left. , -1.14E3, \begin{bmatrix} -1.77 & 484.9 \\ -484.9 & -1.77 \end{bmatrix}, \begin{bmatrix} -1.38 & 103.86 \\ -103.86 & -1.38 \end{bmatrix}, -153.25 \right).
\end{aligned}
\tag{A.1}
$$